AIMS *Energy*

Research article

Theoretical analysis and mathematical modeling of a solar cogeneration system in Morocco

Saad Eddin Lachhab*, A. Bliya, E. Al Ibrahmi and L. Dlimi

Laboratory of Renewable Energies and Environment, Faculty of Sciences, Ibn Tofail University, BP. 133. 14000-Kenitra, Morocco

* Correspondence: Email: saadeddinlachhab0@gmail.com; Tel: +212637030707.

Abstract: This article is part of a theoretical study based on the mathematical analysis of the new technology of solar cogeneration using the parabolic trough concentrator and the photovoltaic cell. Our main objective is to study the thermal performance of the parabolic cylindrical concentrator in the Rabat-Salé-Kénitra region of Morocco. The methodology is based on solving the energy balance equation of the thermal collector whose elements are the absorber, glass and fluid. The performance of these equations is obtained by the Runge Kutta (RK4) method based on experimental data extracted from the PVGIS software. The numerical solution is found by the Matlab code. The validation test is verified on the studied region of Rabat-Salé-Kénitra. The results of the comparison between the numerical solution and the experimental data corresponding to the different temperature of the thermal collector are encouraging. Finally the thermal performance of the collector is satisfied.

Abbreviations: CSP: Concentrated Solar Power; PV: Photovoltaic; PDE: Partial Differential Equations; PVGIS: Photovoltaic Geographical Information System; SHW: Solar Hot Water; HTF: Heat Transfer Fluid

1. Introduction

The world has experienced significant economic development for more than a century. The industrial development incarnated particularly by the increase of the car fleet and the multiplication of domestic equipment have provoked a significant increase in energy demand. This makes clean

energy a key theme in the climate change debate. The major part of this is concentrated on the electricity production. Indeed, incident solar radiation is focalized on the photovoltaic panels [1–2] as well as the Concentrated Solar Power (CSP) of the form parabolic cylindrical.

Solar cogeneration [3–5] is a tool that combines PV photovoltaic and SHW thermal converter technology [6]. This new system is profitable at the level of energy production and respects of the environment on another side. This optimized system has a commercial advantage [7] at the level of electrical energy.

Cogeneration is the simultaneous production of two different forms of energy from the same resource. The most common application of this system is the heat produced during the production of energy recovered both by a heat exchanger, which can then be used to produce steam in order to produce electrical energy.

Literature studies on solar cogeneration have shown that it provides about five times the energy of a photovoltaic system in the same region. Also, they show that solar cogeneration could improve the performance of the solar concentrator, based on exploit of the solar rays lost by the parabolic cylindrical concentrator. In other words, when the solar radiation reflects by the mirror reaches the lower surface of the parabolic collector tube, in addition to this geometric losses that lead to a decrease in the effective area of solar capture. The parabolic cylindrical solar concentrator can reach a thermal efficiency [8] of 75% in better conditions. In contrast the photovoltaic systems have an electrical efficiency [9] of up than 15%. The combination of the solar concentration system and photovoltaic cells in a single system allows modification of the power electricity production and increase the global efficiency about 90%. More importantly, the total economic value of the energy provided by a solar cogeneration system is more than twice superior to that of a photovoltaic system used in California [10,11] for example.

The adoption of renewable energy technologies as a sustainable development in Morocco forms an essential approach in scientific research in the field of energy production technologies, especially technologies that produce energy respects of the environment.

Solar cogeneration is considered one of the best solution for converting solar energy to dual thermal and electrical energy. On the other hand solar energy is becoming one of the most promising sources of energy. Several developing countries with high exposure to solar radiation are now moving towards concentration of solar energy for electricity, particularly in Morocco[12]. Parabolic solar collector [13] can reach a temperature of up to 400 °C and depends mainly on the concentration rate of solar radiation.

This article presents a detailed numerical model. It allows to develop the performances of a solar parabolic trough collector in the context of solar cogeneration. This technique optimizes the development design of the CSP-PV collector for solar cogeneration, especially in terms of temperature distribution on all components of the thermal collector. We have simplified a set of equations describing the energy balance at the level of the studied system. These equations are numerous and complex because of the multiplicity of various heat transfer factors. There are many numerical methods that discrete the different temperature distributions of the thermal system (glass-absorber-fluid). Considering the performance of the RK4 method in numerical resolution, we adopted it in our case. So the numerical results are interested in the three thermal profiles which are the temperature of the fluid T_f and the glass T_{gl} and the absorber T_m. The validation of this model is presented on the region of Rabat-Salé-Kenitra which is located in the north of Morocco. For this, we are based on PVGIS software to calculate the incident radiation and ambient temperature over the studied region. The results obtained are well illustrated at the end of this article.

1.1. Description of solar cogeneration sensor operation

The solar cogeneration approach combines proven photovoltaic (PV) and hot water solar (SHW) technologies into a single integrated system that maximizes the incident energy from the sun.

The proposed figure 1 corresponds to a small lateral section of a solar concentrator [14–15] that conducts solar radiation towards a centre composed of a cylindrical tube and a photovoltaic cell [16]. For maintain solar radiation at the fixed focal point, we use a tracking system which has two axes consisting of two mechanisms. The first is for tracking daily, he moves the reflector on a mobile support in proportion to the solar declination and the other depends on the time provides the rotation of the reflector in a shape synchronized with the movement of the sun during the day. This movement of the reflector concentrates the solar radiation in a receiving cavity of our system.
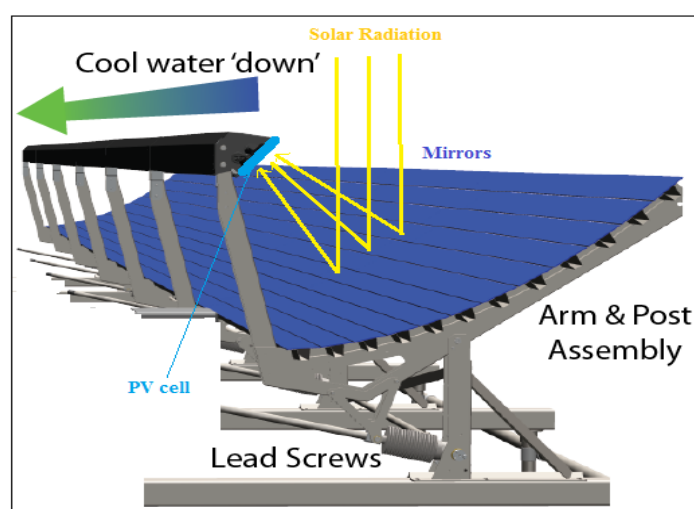
Figure 1. Solar cogeneration.

The main components of a single solar cogeneration module, Figure 1, are as follows:

Receiver: This is the energy-collection device. It consists of a PV cell bonded to a heat exchanger assembly, and includes hydronic and electrical connections. Coolant flows through passages in the plate to provide hot water.

Mirrors: The mirrors are arranged in twelve rows. Each one consists of glass mirrors bonded to a galvanized steel support element.

Arm & Post: The primary support structure for the system. The post is bolted to the rack. The arm pivots on the post to provide the tracking function. The straight member of the arm holds the receiver. The curved portion of the arm holds the mirrors. The Arm & Post assembly also includes the gear drive and lead screw for the tracking mechanism.

2. Mathematical formulation of heat transfer tubes

Mathematical modeling of heat transfer at the level of collectors solar parabolic (CSP) has been explored by many authors [17].The modeling principle is based on an energy balance between the essential elements of the heat sensor and the heat transfer fluid. Figure 2 shows a part transversal of

heat transfer tube containing three components (glass, absorber, fluid) between the receiving tube and the heat transfer fluid and their environment.
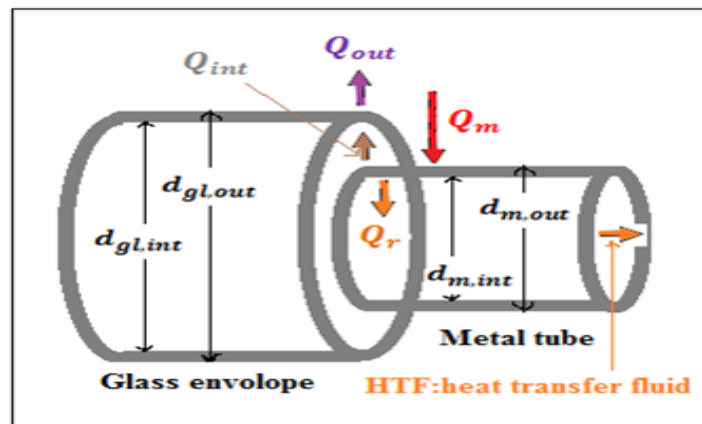
Figure 2. Scheme of the different thermal exchanges of the HTF.

This part focuses on modeling the thermal equation based on the treatment of the different temperatures of our system (glass, absorber, fluid) [18]. The following assumptions are considered:
-The regime is transitional.
-The form of the parabola is symmetrical.
-The temporal variations in absorber thickness are negligible.
-The conduction exchange in the absorber is negligible.
-The effect of the absorber shadow on the mirror is negligible.
-The solar flux at the absorber is uniformly distributed.
-The solar radiation is constant.
-The flow of the fluid is one-dimensional and homogeneous fluid (water) with a constant mass flow rate.
-The dimension of the heat transfer tube is 6 meters long and has an external radius of $d_{gl.out} = 0.120$ mm and an internal radius of $d_{gl.int} = 0.129$ mm. For absorber with an external radius of $d_{m.out} = 0.110$ mm and an internal radius of $d_{m,int} = 0.118$ mm.

2.1. Energy balance for the fluid

The state variables we consider are the fluid temperature T_f, the absorber tube T_m and the glass envelope T_{gl}. The energy balance of the heat recovery element leads to three partial differential equations, consisting of three temperatures. The first equation describes the fluid temperature T_f. It depends on the (weather) time t and the space x. The second and third equation describing the temperature of the absorption tube T_m and the temperature of the glass envelope. The energy balance of the fluid circulating in the inside tube is expressed by the following transient equation.

$$\rho_f C_f . A_f \frac{\partial T_f}{\partial t}(x.t) + \rho_f C_f . \frac{\dot{V}_f}{N_{col}} \frac{\partial T_f}{\partial x}(x.t) = Q_r(x.t) \tag{1}$$

$Q_r(x.t)$ Represents a heat transfer by convection between the cylindrical absorber tube and the fluid circulating inside the absorber by unit length. It is given by the formula (2) in which $h_{m.f}$ is the coefficient of heat transfer by convection between the metal tube and the fluid, $A_{surf.m.int}$ is the inside surface by length of the metal tube.

$$Q_r(x.t) = h_{m.f}A_{surf.m.int}\left(T_m - T_f\right) \tag{2}$$

According to the approximations chosen before the equation (1), Equations (3) and (4) will be simplified using α constant depends on the fluid equation. In general the variation of the energy transfer in the heat transfer fluid is given by:

$$\frac{\partial T_f}{\partial t}(x.t) = \underbrace{\frac{h_{m.f}A_{surf.m.int}}{\rho_f C_f.A_f}}_{\alpha_{11}}\left(T_m - T_f\right) \tag{3}$$

$$\Longrightarrow \quad \frac{\partial T_f}{\partial t}(x.t) = \alpha_{11}\left(T_m - T_f\right) \tag{4}$$

Equation (4) presents a first-order differential equation describing the variation in fluid temperature as a function of time and the absorber.

2.2. Energy balance for the absorber

The energy balance of the absorber is given by the following formula in equation (5):

$$\rho_m C_m.A_m \frac{\partial T_m}{\partial t}(x.t) = Q_{sol_{sol}}^{abs}(x.t) - Q_{int}(x.t) - Q_r(x.t) \tag{5}$$

$Q_{sol_{sol}}^{abs}(x.t)$: The amount of solar energy absorbed by the solar collector of parabolic cylindrical form dependent on of time and sensor properties and is defined by:

$$Q_{sol_{sol}}^{abs}(x.t) = I_s F(cos\theta)D_{eff}\eta_{opt}\gamma \tag{6}$$

Or I_s Solar Direct irradiance, $F(cos\theta)$ Incidence modifier function θ represents angle of incidence degree, D_{eff} effective width of the collector, η_{opt} optical efficiency and γ factor depending of dirt on the mirrors.

Between the two concentric tubes (metal and glass) there's the exchange of heat by conduction and radiation [19]. He depends on of the various characteristics of stainless steel and glass.

$$Q_{int}(x.t) = Q_{int}^{rad}(x.t) + Q_{int}^{conv}(x.t) \tag{7}$$

$$= \frac{\sigma A_{surf.m.out}\left(T_m^4 - T_{gl}^4\right)}{\dfrac{1}{\varepsilon_m} + \dfrac{1-\varepsilon_{gl}}{\varepsilon_{gl}}\dfrac{d_{m.out}}{d_{gl.int}}} + \frac{2\pi k_{eff,air}\left(T_m - T_{gl}\right)}{\ln\left(\dfrac{d_{gl,int}}{d_{m,out}}\right)} \tag{8}$$

Modeling the heat transfer equation at the absorber level is more difficult and complicated. The absorber depends on a large number of variable and different parameters. We will try to assemble the

formulas (8), (6) and (2) in only equation differential (9). Subsequently, we will develop this equation based (10) and (11) to obtain a simple equation homogeneous (12) and describing the temperature T_m at the level of the cylindrical collector.

$$\rho_m C_m . A_m \frac{\partial T_m}{\partial t}(x.t) = I_s F(\cos\theta) D_{eff} \eta_{opt} \gamma - \frac{\sigma A_{surf.m.out}\left(T_m^4 - T_{gl}^4\right)}{\frac{1}{\varepsilon_m} + \frac{1 - \varepsilon_{gl}}{\varepsilon_{gl}} \frac{d_{m.out}}{d_{gl.int}}}$$

$$- \frac{2\pi k_{eff,air}\left(T_m - T_{gl}\right)}{\ln\left(\frac{d_{gl,in}}{d_{m,out}}\right)} - h_{m.f} A_{surf.m.int}\left(T_m - T_f\right) \tag{9}$$

$$\Rightarrow \quad \frac{\partial T_m}{\partial t}(x.t) = \frac{I_s F(\cos\theta) D_{eff} \eta_{opt} \gamma}{\rho_m C_m . A_m} - \frac{\sigma A_{surf.m.out}}{\left(\frac{1}{\varepsilon_m} + \frac{1 - \varepsilon_{gl}}{\varepsilon_{gl}} \frac{d_{m.out}}{d_{gl.int}}\right)\rho_m C_m . A_m}\left(T_m^4 - T_{gl}^4\right)$$

$$- \frac{2\pi k_{eff,air}}{\ln\left(\frac{d_{gl,in}}{d_{m,out}}\right)\rho_m C_m . A_m}\left(T_m - T_{gl}\right) - \frac{h_{m.f} A_{surf.m.int}}{\rho_m C_m . A_m}\left(T_m - T_f\right) \tag{10}$$

$$\Rightarrow \quad \frac{\partial T_m}{\partial t}(x.t) = \underbrace{\frac{I_s F(\cos\theta) D_{eff} \eta_{opt} \gamma}{\rho_m C_m . A_m}}_{\psi} + \underbrace{\frac{h_{m.f} A_{surf.m.int}}{\rho_m C_m . A_m}}_{\alpha_{12}} T_f$$

$$- \underbrace{\left(\frac{\sigma A_{surf.m.out}}{\left(\frac{1}{\varepsilon_m} + \frac{1 - \varepsilon_{gl}}{\varepsilon_{gl}} \frac{d_{m.out}}{d_{gl.int}}\right)\rho_m C_m . A_m}\right)}_{\alpha_{21}} T_m^4 - \underbrace{\left(\frac{2\pi k_{eff,air}}{\ln\left(\frac{d_{gl,in}}{d_{m,out}}\right)\rho_m C_m . A_m} + \frac{h_{m.f} A_{surf.m.int}}{\rho_m C_m . A_m}\right)}_{\alpha_{22}} T_m$$

$$+ \underbrace{\left(\frac{\sigma A_{surf.m.out}}{\left(\frac{1}{\varepsilon_m} + \frac{1 - \varepsilon_{gl}}{\varepsilon_{gl}} \frac{d_{m.out}}{d_{gl.int}}\right)\rho_m C_m . A_m}\right)}_{\alpha_{31}} T_{gl}^4 + \underbrace{\left(\frac{2\pi k_{eff,air}}{\ln\left(\frac{d_{gl,in}}{d_{m,out}}\right)\rho_m C_m . A_m}\right)}_{\alpha_{32}} T_{gl} \tag{11}$$

According to this long theoretical demonstration could developed the energy balance on the absorber under the following equation (12).

$$\Rightarrow \quad \frac{\partial T_m}{\partial t}(x.t) = \psi + \alpha_{12} T_f - \alpha_{21} T_m^4 - \alpha_{22} T_m + \alpha_{31} T_{gl}^4 + \alpha_{32} T_{gl} \tag{12}$$

This equation allows us to predict a heat transformation mechanism with parameters related to the characteristic of the metal used. These characteristics are emissivity, absorptivity and transmission factors. Another important factor in this equation is the solar radiation received on a given conduit surface.

2.3. Energy balance of the glass

In the following, we continue to treat the energy balance that transforms solar energy between atmosphere and glass [20]. There are the transformation by conduction and radiation between the air and glass envelope. For this we have obtained the formula (13) which presents a first order differential equation.

$$\rho_{gl}.C_{gl}.A_{gl}\frac{\partial T_{gl}}{\partial t}(x.t) = Q_{int}(x.t) - Q_{out}(x.t) \tag{13}$$

A quantity of thermal energy is exchanged by convection and radiation between the glass envelope and the environment. This thermal energy [21] is defined by the characteristics of the glass and by those defining ambient air as follows:

$$Q_{out}(x.t) = Q_{out}^{rad}(x.t) + Q_{out}^{conv}(x.t) \tag{14}$$

$$= \sigma\varepsilon_{gl}A_{surf.gl.out}(T_{gl}^4 - T_{amb}^4) + \sigma h_{gl.amb}A_{surf.gl.out}(T_{gl} - T_{amb}) \tag{15}$$

After, the possibility of replacing formulas (8) and (15) in the energy equation (13) and after the division by quantity $\rho_{gl}.C_{gl}.A_{gl}$ we obtain a system of partial differential equations (PDE) which can be rewritten in the following form.

$$\Rightarrow \quad \rho_{gl}.C_{gl}.A_{gl}\frac{\partial T_{gl}}{\partial t}(x.t) = \frac{\sigma A_{surf.m.out}(T_m^4 - T_{gl}^4)}{\frac{1}{\varepsilon_m} + \frac{1-\varepsilon_{gl}}{\varepsilon_{gl}}\frac{d_{m.out}}{d_{gl.int}}} + \frac{2\pi k_{eff,air}(T_m - T_{gl})}{\ln\left(\frac{d_{gl,int}}{d_{m,out}}\right)}$$

$$-\sigma\varepsilon_{gl}A_{surf.gl.out}(T_{gl}^4 -) - \sigma h_{gl.amb}A_{surf.gl.out}(T_{gl} - T_{amb}) \tag{16}$$

$$\Rightarrow \quad \frac{\partial T_{gl}}{\partial t}(x.t) = \underbrace{\left(\frac{\sigma A_{surf.m.out}}{\left(\frac{1}{\varepsilon_m} + \frac{1-\varepsilon_{gl}}{\varepsilon_{gl}}\frac{d_{m.out}}{d_{gl.int}}\right)\left(\frac{1}{\rho_{gl}.C_{gl}.A_{gl}}\right)}\right)}_{\beta_{11}}T_m^4 +$$

$$\underbrace{\left(\frac{1}{\rho_{gl}.C_{gl}.A_{gl}}\right)\left(\frac{2\pi k_{eff,air}}{\ln\left(\frac{d_{gl,int}}{d_{m,out}}\right)}\right)}_{\beta_{12}}T_m - \underbrace{\left(\frac{\sigma A_{surf.m.out}}{\left(\frac{1}{\varepsilon_m} + \frac{1-\varepsilon_{gl}}{\varepsilon_{gl}}\frac{d_{m.out}}{d_{gl.int}}\right)\left(\frac{1}{\rho_{gl}.C_{gl}.A_{gl}}\right)} + \frac{\sigma A_{surf.gl.out}}{\rho_{gl}.C_{gl}.A_{gl}}\right)}_{\beta_{21}}T_{gl}^4$$

$$+ \underbrace{\left(\frac{\sigma\varepsilon_{gl}A_{surf.gl.out}}{\rho_{gl}.C_{gl}.A_{gl}} + \frac{\sigma h_{gl.out}A_{surf.gl.out}}{\rho_{gl}.C_{gl}.A_{gl}}\right)}_{\beta_{22}}T_{gl}$$

$$+ \underbrace{\left(\frac{\sigma\varepsilon_{gl}A_{surf.gl.out}}{\rho_{gl}.C_{gl}.A_{gl}}\right)}_{\beta_{31}}T_{amb}^4 + \underbrace{\left(\frac{\sigma h_{gl.amb}A_{surf.gl.out}}{\rho_{gl}.C_{gl}.A_{gl}}\right)}_{\beta_{32}}T_{amb} \tag{17}$$

$$\Rightarrow \quad \frac{\partial T_{gl}}{\partial t}(x.t) = \beta_{11}T_m^4 + \beta_{12}T_m + \beta_{21}T_{gl}^4 + \beta_{22}T_{gl} + \beta_{31}T_{amb}^4 + \beta_{32}T_{amb} \tag{18}$$

The parameters α_{ij} and β_{ij} are constant depends on the nature of the system and also the characteristics of the fluid used as well as the ownership of the envelope and the glass absorber. On the other hand they are taking into account of the ambient temperature T_{amb} which is a constant factor. Finally we arrive to optimize the energy balance of a part of the cylindrical length of solar concentrator under the equation (19).

$$\frac{\partial}{\partial t}\begin{pmatrix} T_f \\ T_m \\ T_{gl} \end{pmatrix} = \psi + \begin{pmatrix} -\alpha_{11} & \alpha_{11} & 0 \\ \alpha_{12} & -\alpha_{22} & \alpha_{32} \\ 0 & \beta_{12} & \beta_{22} \end{pmatrix}\begin{pmatrix} T_f \\ T_m \\ T_{gl} \end{pmatrix} + \begin{pmatrix} 0 & 0 & 0 \\ 0 & -\alpha_{21} & \alpha_{31} \\ 0 & \beta_{11} & \beta_{21} \end{pmatrix}\begin{pmatrix} T_f^4 \\ T_m^4 \\ T_{gl}^4 \end{pmatrix} + \beta_{31}T_{amb}^4$$
$$+ \beta_{32}T_{amb} \tag{19}$$

The disposition of the equations (4) and (12) and (18) in a single formula (19) has allowed us to have a matrix that possesses 3 variables (T_f, T_m, T_{gl}) describing the evolution of energy over time under a first-order differential equation.

2.4. Efficiency of solar cogeneration

Another important parameter that examines the total efficiency of the thermal collector CSP-PV is given by the sum of the thermal efficiency [22] of the parabolic trough concentrator η_{the} and the electrical efficiency of the photovoltaic collector (η_{ele}).

$$\eta = \eta_{the} + \eta_{elec} \tag{20}$$

With η_{the} is the thermal efficiency that can be calculated using formula (21). The thermal efficiency of the solar concentrator represents the ratio between the useful power and the incident power received by the lower surface of the solar concentrator tube. It is expressed as the ratio of the useful power to the solar energy.

$$\eta_{th} = \frac{Q_r(x.t)}{SG} = \frac{h_{m.f}A_{surf.m.int}(T_m - T_f)}{SG} \tag{21}$$

Electrical efficiency η_{ele} is the ratio between the electrical power of the PV cell [23] and the amount of solar energy received.

$$\eta_{ele} = \frac{P_{pv}}{GA_{eff}} \tag{22}$$

Or P_{pv} = Electrical power in the PV panel (W)
A_{eff} = Effective area of the PV panel (m^2) and G = solar irradiation, otherwise known as light power received per unit area (W / m^2).

2.5. Mathematical process resolution

There are different numerical methods to solve mathematical equations describing the energy balance of a solar concentrator. In our case we are interested in solving the differential equation presented in the matrix (19) by the Runge Kutta method of order 4 [24]. For this, the method requires many more steps to obtain results and the calculating time depends on accuracy or defined time step. Moreover, the Runge-Kutta method is among the family of iterative methods in which, from a desired order of coherence, a quadrature or digital integration algorithm is established to solve the problem in as few steps as possible .The choice of one algorithm or another will give rise to the different Runge-Kutta methods. The theoretical principle of these methods lies on the application of the fundamental theorem of computation to the differential equation of the problem of the initial value. By doing this, we can define the solution to the problem as the sum of the initial condition plus a definite integral, which we will solve later using a numerical integration method. The mathematical process is as follows:

$$y(t_{k+1}) = y(t_k) + h \sum_{i=1}^{r} a_i * f\left(t_{k,i}, y(t_{k,i})\right) \tag{23}$$

Where h is the laps between iterations (t_{k+1}, t_k), a_i are the coefficients of the method used and r the number of steps of the method. For the evaluation of the intermediate points, the numerical solution of the definite integral will be applied again and conduct to the following result:

$$y(t_{k+1}) = y(t_k) + h \sum_{i=1}^{j-1} b_{i,j} * f\left(t_{k,j}, y(t_{k,j})\right) \tag{24}$$

Determining the three defined coefficients, the weights of the different steps a_i, the spacing of the subintervals serving as support for the method c_i and the weights of the nodes in the estimation of the intermediate points $b_{i,j}$. To define the method, one usually uses a matrix[25] of coefficients which marks the algorithm of the same one, in the following way

$$\begin{pmatrix} c_1 & 0 & 0 & \dots & 0 \\ c_2 & b_{21} & 0 & \dots & 0 \\ \vdots & \vdots & \ddots & \ddots & \vdots \\ c_r & br_1 & br_2 & \dots & 0 \\ & a_1 & a_2 & \dots & a_r \end{pmatrix} \tag{25}$$

2.6. Resolution of the problem using the Runge-Kutta 4th order method

This method is, in the family of Runge-Kutta methods, probably the most used. At this point it is sometimes called directly as Runge-Kutta method. This method is an explicit method of four steps which the minimum necessary to reach the fourth order. The coefficient matrix associated with it is as follows:

$$\begin{pmatrix} 0 & 0 & 0 & 0 & 0 \\ \dfrac{1}{2} & \dfrac{1}{2} & 0 & 0 & 0 \\ \dfrac{1}{2} & 0 & \dfrac{1}{2} & 0 & 0 \\ 1 & 0 & 0 & 1 & 0 \\ & \dfrac{1}{6} & \dfrac{2}{6} & \dfrac{2}{6} & \dfrac{1}{6} \end{pmatrix} \tag{26}$$

The characteristics mentioned are observed in the matrix, the four stages of the process as a function of the dimensions of the matrix coefficient $b_{i,j}$ and the fact of being explicit of the zero value of the coefficients of the main and upper diagonal of this one.

Finally, to obtain the value at the iteration point, the four steps will be taken into account, by weighting the central nodes with twice the weight of the end nodes. However, the particular scheme of the method will be the following:

$$y(t_{n+1}) = y(t_n) + \frac{h}{6}(k_1 + 2k_2 + 2k_3 + k_4) \tag{27}$$

And to compute the k-values, which are only the values of the subdivision point estimate in the four steps performed, we would have the following configuration (where we will substitute the comfort and clarity of the writing and (t_n) for y_n directly.

$$\begin{cases} k_1 = f(t_n, y_n) \\ k_2 = f\left(t_n + \dfrac{h}{2}, y_n + \dfrac{h}{2}k_1\right) \\ k_3 = f\left(t_n + \dfrac{h}{2}, y_n + k_2\right) \\ k_4 = f(t_n + h, y_n + hk_3) \end{cases} \tag{28}$$

To solve the problem of the initial value, it would be necessary to enter the initial conditions expressed at the end of the simulation interval equivalent to t = 0. In our case, the initial conditions are the same for all the variables $T_m^0 = T_{gl}^0 = T_f^0 = T_a^0 = 25° \, ℃$

$$\frac{\partial}{\partial t}\begin{pmatrix} T_f \\ T_m \\ T_{gl} \end{pmatrix} = \psi + \begin{pmatrix} -\alpha_{11} & \alpha_{11} & 0 \\ \alpha_{12} & -\alpha_{22} & \alpha_{32} \\ 0 & \beta_{12} & \beta_{22} \end{pmatrix}\begin{pmatrix} T_f \\ T_m \\ T_{gl} \end{pmatrix} + \begin{pmatrix} 0 & 0 & 0 \\ 0 & -\alpha_{21} & \alpha_{31} \\ 0 & \beta_{11} & \beta_{21} \end{pmatrix}\begin{pmatrix} T_f^4 \\ T_m^4 \\ T_{gl}^4 \end{pmatrix} + \beta_{31}T_{amb}^4$$
$$+ \beta_{32}T_{amb} \tag{29}$$

From this initial problem, the simulation interval and the number of iterations to be performed or the passage of the nodes are fixed. The schema to use for each iteration will be the following, in our case applied to a system of 3 differential equations.

$$
\begin{cases}
T_f^{i+1} = T_f^i + \dfrac{1}{6}\left(k_{f1} + 2k_{f2} + 2k_{f3} + k_{F4}\right) \\[2mm]
T_m^{i+1} = T_m^i + \dfrac{1}{6}\left(k_{m1} + 2k_{m2} + 2k_{m3} + k_{m4}\right) \\[2mm]
T_{gl}^{i+1} = T_{gl}^i + \dfrac{1}{6}\left(k_{gl1} + 2k_{gl2} + 2k_{gl3} + k_{gl4}\right)
\end{cases}
\tag{30}
$$

With this study, we will be able to determine the time evolution of significant collector temperatures throughout the simulation interval. Although, the following considerations should be taken into account, with the k defines as following:

$$
\begin{cases}
k_{f1} = h * f_f\left(t_i, T_f^i\right) \\[2mm]
k_{f2} = h * f_f\left(t_{i,} + \dfrac{h}{2}, T_f^i + \dfrac{k_{f1}}{2}\right) \\[2mm]
k_{f3} = h * f_f\left(t_{i,} + \dfrac{h}{2}, T_f^i + \dfrac{k_{f2}}{2}\right) \\[2mm]
k_{f4} = h * f_f\left(h, T_f^i + k_{f3}\right)
\end{cases}
\tag{31}
$$

$$
\begin{cases}
k_{m1} = h * f_m\left(t_i, T_m^i\right) \\[2mm]
k_{m2} = h * f_m\left(t_{i,} + \frac{h}{2}, T_m^i + \frac{k_{m1}}{2}\right) \\[2mm]
k_{m3} = h * f_m\left(t_{i,} + \frac{h}{2}, T_m^i + \frac{k_{m2}}{2}\right) \\[2mm]
k_{m4} = h * f_m\left(h, T_m^i + k_{m3}\right)
\end{cases}
\tag{32}
$$

$$
\begin{cases}
k_{gl1} = h * f_{gl}\left(t_i, T_m^i\right) \\[2mm]
k_{gl2} = h * f_{gl}\left(t_{i,} + \dfrac{h}{2}, T_m^i + \dfrac{k_{m1}}{2}\right) \\[2mm]
k_{gl3} = h * f_{gl}\left(t_{i,} + \dfrac{h}{2}, T_m^i + \dfrac{k_{m2}}{2}\right) \\[2mm]
k_{gl} = h * f_{gl}\left(h, T_{gl}^i + k_{gl}\right)
\end{cases}
\tag{33}
$$

With this scheme, we will be able to determine the temporal evolution of the significant temperatures of the collector [26] during the whole simulation interval. For this, the following considerations should be taken into account.

We have previously said that in differential equations, all parameters that were not variables should be computed before and considered as coefficients. However, some of these components depend on the time or temperature of some of the evaluated components, such as the ambient temperature in the first case or the film coefficient between the hood and the photovoltaic plate in the second. The relationship of dependence of these parameters with the evaluated variables must be introduced into the differential equation by substitution, in order not to create approximation failures and to respect the principle of the model making it possible to evaluate all the coefficients in real time.

We typically need some inputs for the algorithm:

-A range that we want to do the calculations over:, $a \leq t \leq b$ let's use a=0, b=1

- The number of steps N, say N=10

- The step size h=(b−a)/N=1/10=0.1

2.7. Average daily solar irradiance for region (Rabat-Salé-Kenitra) of Morocco

In our research we can not talk about thermal or photovoltaic technology without solar irradiation. In our case of Morocco's Rabat-Salé-Kenitra has a high interesting geographical position. Thus it's an opportunity to examine the reliability of our theoretical study. The solar radiation data were obtained from measurements of the European satellite PVGIS [27–29] with metrological parameters on the zone of the location 34°01'53.34"north, 6°50'39.72"west, and elevation: 139 m. Optimal inclination angle is: 31 degrees.
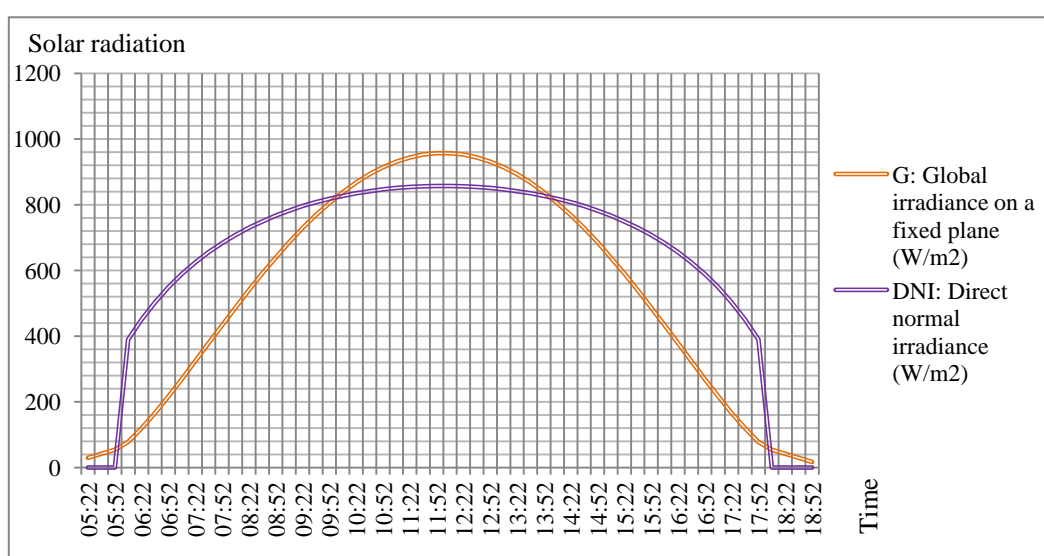
Figure 3. Estimated by PVGIS of average daily solar irradiance for region (Rabat-Salé-Kenitra) of Morocco.

The figure 3 shows clearly from the sunrise that the flow of solar energy begins to increase until reaching its maximum value at 11: 37: 00 and it continues to keep this value until 14: 37: 00. After this time, it starts to go down until the sunset. These parameters help us to validate and initialize the initial parameters necessary of our solar cogeneration system. So we can examine and solve our matrix in an efficient way.

3. Resultants and discussions

### 3.1. Comparison between the analytical and the numerical

Figure 4 shows a comparison between the two temperatures at outlet of the fluid. One temperature is calculated by using the method of RK4 ran on the Matlab, the other one is derived from the experimental data. The figure 3 is an inlet data to run our program. The curves obtained are

fairly identical in the way of their evolution. The difference of the temperature's values varies slightly from the sunrise to de sunset. It reaches the maximum at de midday (between 11 h 22 min inlet 14 h 22).The explanation is possible due to the daily variation coefficient of reflection and emission either of the fluid or of the wall pipe and also of the coefficient absorber [30–32].
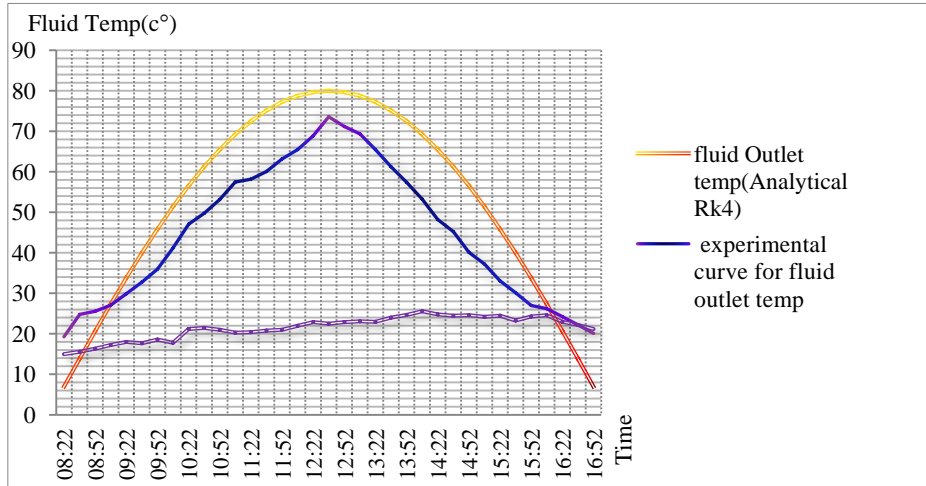
Figure 4. Fluid outlet temperature.

3.2. Theoretical absorber temperature Rk4
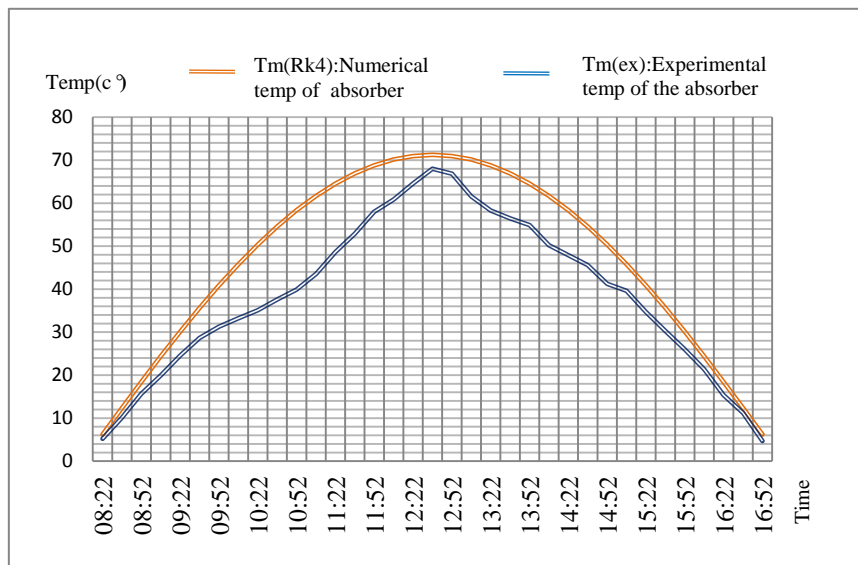
**Figure 5.** Variation absorber's temperature.

A good match between experimental temperatures and theoretical temperatures attests a good description of the phenomena and interactions occurring during the operation of the system. Moreover on the lower part which faces the mirror of the CSP, the flow is concentrated. For the upper part, the density of the thermal flux is very low because on this part the radiation which touches the face is a direct radiation that has been proposed in the boundary conditions.

In the same way, the figure 5 shows the temperature evolution of the absorber. The two curves obtained by numerical RK4 and by the experimental data show the same evolution of the figure 4. We add that the difference value between the two curves is week at the sunrise as well as at the sunset. We note that this difference increase after the sunrise until before the beginning of midday. The same difference is noted after midday until sunset. The difference value can be explained by the estimation of the absorption coefficient by the RK4.

3.3. Theoretical glass temperature Rk4

When we look at the evaluation of the glass's temperature, the figure 6 shows a good agreement between the two methods Runge Kutta 4 and experimental data. The two curves are mainly too closed at the sunrise as well as at the sunset. Slightly a way the sunrise until the midday, the two curves are too closed than after midday. This differences can be explained by an over estimation of the transmission coefficient of the glass. This difference is more marked after the midday when the ambient temperature reaches the maximum value.

So the glass well be more hot and it is continued to be hot after midday. This can be influenced the evaluation of the transmission coefficient.
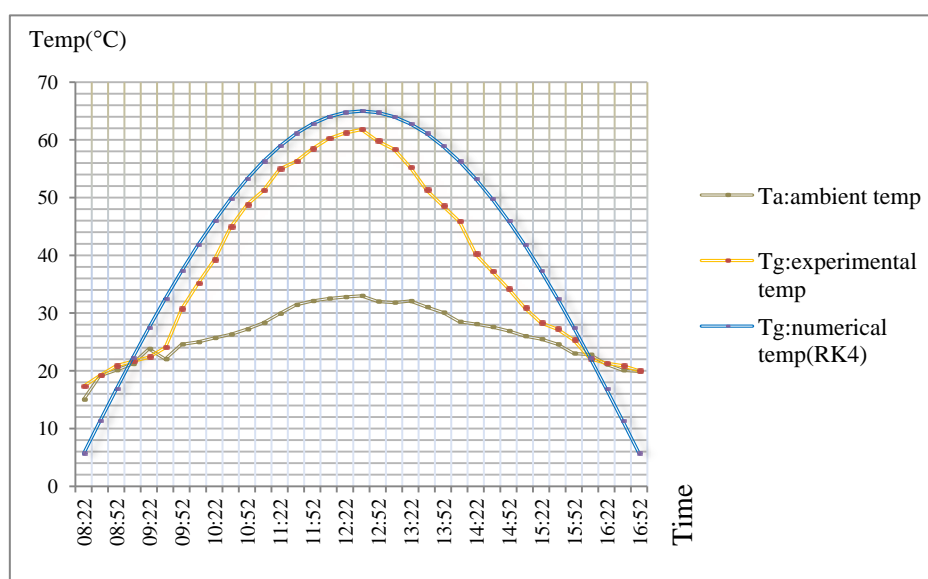
Figure 6. Variation glass's temperature.

3.4. Efficiency for CSP

The experimental and simulation analysis of the CSP's efficiency determined by the equations (21) and (22) are well represented in the figure 7. The evolution by the time of the CSP thermal efficiencies modeled by the Runge Kutta method and the experimental thermal efficiencies show a good agreement except at the midday and from 11 h 22 to 15 h 00. At the interval time when the numerical and theoretical efficiencies are identical, the temperature values estimated before are well before midday until afternoon. The difference of efficiencies between the two methods is also reinforced the errors observed between the temperature mentioned in figure above.
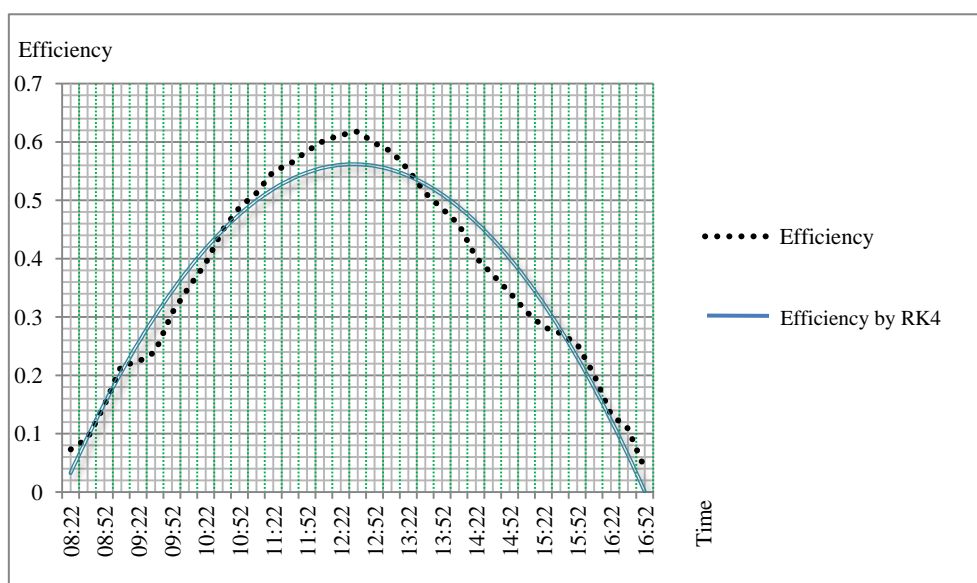
Figure 7. Modelled energy efficiency of CSP.

4. Conclusion

This paper proposes the study of a solar cogeneration system that consists of a concentrated solar system (CSP) and photovoltaic's (PV). The object of describing this new technology is to highlight its importance in the field of renewable energies. For this reasons, it can simultaneously produce thermal and electrical energy. In this work, we focused on the theoretical study of heat transfer on a 6-metre long part of the tube. We have demonstrated the energy balance of the components (glass-absorber-fluid). A set of differential equations, have been very long and complex in a matrix of three variables (T_f, T_m, T_{gl}). According to this matrix we solved this system using the Rk4 method. The region of the (Rabat-salé-kenitra) of our Moroccan country was our space to test this study. For this, we have modeled a calculation code from the Matlab software we used. The results obtained show the influence of the simplification of the differential system on the performance and efficiency of the solar concentrator. As well, these results encourage us to develop our research to increase the electricity and heat rate based on the solar cogeneration system.

Conflict of interest

The authors declare no conflicts of interest in this paper.

References

1. Hoffmann W (2006) PV solar electricity industry: market growth and perspective. *Sol Energ Mat Sol C* 90: 3285–3311.
2. Caluianu IR, Băltăreţu F (2012) Thermal modelling of a photovoltaic module under variable free convection conditions. *Appl Therm Eng* 33: 86–91.

3. Youssef WB, Maatallah T, Menezo C, et al. (2018) Assessment viability of a concentrating photovoltaic/thermal-energy cogeneration system (CPV/T) with storage for a textile industry application. *Sol Energ* 159: 841–851.

4. Sharma KM, Spandana YS, Krishna LN (2015) Generation of hybrid power by wind and solar cogeneration techniques. *International Journal of Scientific Research Engineering and Technology (IJSRET) ISSN: 2278–0882 EATHD-2015 Conference Proceeding*, Jalandhar, India.

5. Nia MH, Nejad AA, Goudarzi AM, et al. (2014) Cogeneration solar system using thermoelectric module and fresnel lens. *Energ convers manage* 84: 305–310.

6. Zhou C, Liang R, Zhang J (2017) Optimization design method and experimental validation of a solar pvt cogeneration system based on building energy demand. *Energies* 10: 1281.

7. Florschuetz LW (1979) Extension of the Hottel-Whillier model to the analysis of combined photovoltaic/thermal flat plate collectors. *Sol Energ* 22: 361–366.

8. Agarwal RK, Garg HP (1994) Study of a photovoltaic-thermal system—thermosyphonic solar water heater combined with solar cells. *Energ Convers Manage* 35: 605–620.

9. Barkaoui AE, Zarhloule Y, Rimi A, et al. (2015) *Proceedings of Geothermal Country Update report of Morocco (2010–2015).*

10. Jiang S, Hu P, Mo S, et al. (2010) Optical modeling for a two-stage parabolic trough concentrating photovoltaic/thermal system using spectral beam splitting technology. *Sol Energ Mat Sol C* 94: 1686–1696.

11. Isotani S, Pontuschka WM, Isotani S (2012) An algorithm to optimize the calculation of the fourth order Runge-Kutta method applied to the numerical integration of kinetics coupled differential equations. *Appl Math* 3: 1583.

12. Chaturvedi DK (2017) *Modeling and simulation of systems using MATLAB and Simulink*, 1 Eds., CRC press.

13. Rosell JI, Vallverdu X, Lechon MA, et al. (2005) Design and simulation of a low concentrating photovoltaic/thermal system. *Energ Convers Manage* 46: 3034–3046.

14. Poullikkas A (2009) Economic analysis of power generation from parabolic trough solar thermal plants for the mediterranean region—a case study for the island of Cyprus. *Renew sust Energ rev* 13: 2474–2484.

15. García-Valladares O, Velázquez N (2009) Numerical simulation of parabolic trough solar collector: improvement using counter flow concentric circular heat exchangers. *Int J Heat Mass Tran* 52: 597–609.

16. Cheng ZD, He YL, Cui FQ, et al. (2014) Comparative and sensitive analysis for parabolic trough solar collectors with a detailed Monte Carlo ray-tracing optical model. *Appl energ* 115: 559–572.

17. Tao YB, He YL (2010) Numerical study on coupled fluid flow and heat transfer process in parabolic trough solar collector tube. *Sol energ* 84: 1863–1872.

18. Kakaç S, Pramuanjaroenkij A (2016) Analysis of convective heat transfer enhancement by nanofluids: single-phase and two-phase treatments. *J Eng Phys Thermophys* 89: 758–793.

19. Dogonchi AS, Ganji DD (2016) Convection–radiation heat transfer study of moving fin with temperature-dependent thermal conductivity, heat transfer coefficient and heat generation. *Appl Therm Eng* 103: 705–712.

20. Verma SK, Tiwari AK (2015) Progress of nanofluid application in solar collectors: a review. *Energ Convers Manage* 100: 324–346.

21. Ganji DD, Ganji SS, Karimpour S, et al. (2010) Numerical study of homotopy-perturbation method applied to Burgers equation in fluid. *Numer Meth Part D E: Int J* 26: 917–930.

22. Ghazouani K, Skouri S, Bouadila S, et al. (2019) Thermal analysis of linear solar concentrator for indirect steam generation. *Energ Procedia* 162: 136–145.

23. Alobaid M, Hughes B, O'Connor D, et al. (2018) Improving thermal and electrical efficiency in photovoltaic thermal systems for sustainable cooling system integration. *J Sustain Dev Energ, Water Environ Syst* 6: 305–322.

24. Belhocine A, Omar W, Zaidi W (2018) Similarity solution and Runge Kutta method to a thermal boundary layer model at the entrance region of a circular tube: the Lév êque Approximation. *Sci mag* 31: 6–18.

25. Colella P, Dorr MR, Wake DD (1999) A conservative finite difference method for the numerical solution of plasma fluid equations. *J Comput Phys* 149: 168–193.

26. Chiad BT, Kasim NK, Mutlak FAH, et al. (2011) Parabolic trough solar collector–design, construction and testing. *Baghdad Sci J* 8: 658–665.

27. Suri M, Huld T, Dunlop E, et al. (2006) Online data and tools for estimation of solar electricity in Africa: the PVGIS approach. *Proceedings from 21st European Photovoltaic Solar Energy Conference and Exhibition*, Dresden, Germany.

28. Kale PG, Tarai R (2016) Development of rasterized map using PVGIS for assessment of solar PV energy potential of odisha. *Int J Renew Energ Res* 6: 61–73.

29. Kenny RP, Huld TA, Iglesias S (2006) Energy rating of PV modules based on PVGIS irradiance and temperature database. *Proceedings from 21st European Photovoltaic Solar Energy Conference and Exhibition*, Dresden, Germany.

30. Ghodbane M, Boumeddane B (2016) A numerical analysis of the energy behavior of a parabolic trough concentrator. *J Fund Appl Sci* 8: 671–691.

31. Šúri M, Huld TA, Dunlop ED, et al. (2007) Potential of solar electricity generation in the European Union member states and candidate countries. *Sol energ* 81: 1295–1305.

32. Kazemi-Kamyab V, Van Zuijlen AH, Bijl H (2014) Analysis and application of high order implicit Runge–Kutta schemes for unsteady conjugate heat transfer: a strongly-coupled approach. *J Comput Phys* 272: 471–486.

AIMS Press